Magnetic Resonance in Medicine 55:687–693 (2006)

Passive Staining: A Novel Ex Vivo MRI Protocol to Detect Amyloid Deposits in Mouse Models of Alzheimer's Disease

Marc Dhenain,[1]* Benoît Delatour,[2] Christine Walczak,[1] and Andreas Volk[1]

Amyloid plaques are one of the hallmarks of Alzheimer's disease (AD). This study evaluated a novel μMRI strategy based on "passive staining" of brain samples by gadoteric acid. The protocol was tested at 4.7T on control animals and APP/PS1 mice modeling AD lesions. T_1 was strongly decreased in passively stained brains. On high-resolution 3D gradient echo images, the contrast between the cortex and subcortical structures was highly improved due to a T2* effect. The brains of APP/PS1 mice revealed plaques as hypointense spots. They appeared larger in long compared to short TE images. This suggests that, after passive staining, plaques caused a susceptibility effect. This easily performed protocol is a complementary method to classic histology to detect the 3D location of plaques. It may also be used for the validation of in vivo MRI protocols for plaque detection by facilitating registration with histology via post mortem MRI. Magn Reson Med 55:687–693, 2006. © 2006 Wiley-Liss, Inc.

Key words: Alzheimer; amyloid-βpeptide; APP/PS1; mouse; gadolinium; senile plaque

Senile plaques are one of the neuropathological hallmarks of Alzheimer's disease (AD). These microscopic lesions, which are mostly distributed in isocortical and hippocampal brain areas, are extracellular deposits of amyloid-β (Aβ) peptides surrounded by dystrophic neurites (1). The amyloid peptides constituting plaques are misfolded, highly hydrophobic, β sheeted structures (2). Amyloid deposit detection by histology is based on the use of specific dyes or antibodies directed against Aβ epitopes. These methods require slicing of the sample into 2-dimensional sections before staining. Magnetic Resonance Imaging microscopy (μMRI) can be used to perform histologic studies without deconstructing the sample (3). It would be useful to be able to detect amyloid deposits by MR histology in order to evaluate their 3D location without precluding the use of the brain tissue for subsequent histologic analysis. Such an MR protocol should nevertheless be simple and easy to perform for the purpose of routine studies.

Several MRI approaches are currently being evaluated to detect individual amyloid plaques in vivo (4,5). Some results, although not all (6), suggest that amyloid deposits can be detected in post-mortem human brain samples as dark spots, on T2*-weighted (T2*w) images (7). More recent post mortem (8) or in vivo (5,9) studies in aged transgenic mice modeling amyloid deposition were successful in visualizing plaques in T_2- or T2*-weighted images. The deposits appeared as dark spots that were caused by the presence of iron within the amyloid deposits. Unfortunately, because iron accumulation only occurs in aged animals and differentially involves subsets of amyloid plaques (9), this method may not reflect global Aβ load. The difficulties in detecting amyloid by MRI can be partly overcome by the use of targeted contrast agents. To date, most suggested approaches use probes made up of amyloid peptides associated with MR contrast agents (gadolinium chelates or monocrystalline iron oxide nanoparticles (MION)) in conjunction with compounds that allow the contrast agent to cross the blood brain barrier (4,10). These methods are technically difficult and need extensive validation. Ex vivo detection by μMRI should help validation and evaluation of in vivo methods and may also become a complement or even an alternative to classic post mortem histology. Optimization of high resolution ex vivo MRI, preferentially performed at high magnetic field, may be achieved with non specific contrast agents reducing tissue T_1 and, consequently, allowing optimization of the signal to noise ratio per acquisition time. For example, an elegant method, called "active staining" or contrast enhanced MRI, has been developed to improve signal and contrast to noise ratio in post-mortem images from a whole mouse (11) or from excised brain (12). This method is based on the peri-mortem intracardiac perfusion of animals with gadolinium-based contrast agents to decrease tissue T_1.

The aim of our study was to evaluate an easy to perform MR microscopy protocol derived from the active staining method to improve amyloid deposit detection at 4.7 T. Our protocol, called "passive staining," is based on the post-mortem staining of brain samples by gadoteric acid (Dotarem®), a widely used contrast agent. The effect of the staining procedure on contrast and relaxation times was first evaluated on control samples. Then the method was applied to the brains of transgenic mice bearing amyloid pathology, in which we were able to detect plaques.

[1]Integrative Imaging Unit, Curie Institute-INSERM, Centre Universitaire. Laboratoire 112, France.

[2]Laboratoire NAMC, CNRS, UMR 8620, Bāt 446, Université Paris Sud, France.

Grant Sponsors: The Small Animal Imaging Program 2001 (CNRS/INSERM/CEA), the Aging ATC 2002 (INSERM), the Fédération pour la Recherche sur le Cerveau 2003, the Del Duca Fundation, and the ACI Neurosciences (French Research Department).

*Correspondence to: Marc Dhenain, Curie Institute, Centre Universitaire. Laboratoire 112, 91405 Orsay Cedex, France. E-mail: Marc.Dhenain@curie.u-psud.fr

Received 24 May 2005; revised 9 November 2005; accepted 9 November 2005.

DOI 10.1002/mrm.20810

Published online 7 February 2006 in Wiley InterScience (www.interscience.wiley.com).

SUBJECTS AND METHODS

Animals

Experiments were conducted on female APP/PS1 transgenic mice overexpressing amyloid precursor (APP) and presenilin 1 (PS1) mutations associated with familial AD (Double Thy1 APP751 SL (Swedish (KM670/671NL) and London (V717I) mutations introduced in the human APP751 sequence) x HMG PS1 M146L transgenic mouse line (13,14). In these animals, the amyloid deposition starts at the age of 2.5 months (13). Amyloid free female PS1 and wild-type C57BL6 animals were used as controls. The PS1 mice had been backcrossed on a C57Bl6 background for more than 6 generations, whereas the APP mice were on a CBA (12.5%) C57Bl6 (87.5%) background.

Tissue Processing, MRI Experiments, and Image Analysis

MRI studies were performed on a 4.7 Tesla Bruker Biospec 47/30 system, equipped with a 12 cm diameter gradient system (200 mT/m). A surface coil (diameter = 30 mm), actively decoupled from the transmitting birdcage probe (Bruker GmbH), was used for signal acquisition.

Effect of Passive Staining on Relaxation Times

The passive staining protocol consists of soaking a brain (fixed or fresh) in a 1:40 mixture of 0.5 mmol/mL gadoteric acid (Dotarem®, Guerbet, France) and 10% buffered formalin. After this treatment the brain was put in a small Plexiglass container and embedded in a 2.5% agar gel before being imaged by MRI.

The effect of brain immersion in the contrast agent on relaxation times was assessed by measuring T_1, T_2, and T2* in fixed brains from C57BL6 mice before ($n = 2$) and 1, 3, 4, 7, 9, 11, and 16 days after passive staining ($n = 7$). To assess the stability of relaxation times after brain inclusion in agar, T_1, T_2, and T2* were evaluated at least 4 times during a period of 32 h after brain inclusion in the agar gel (on 2 C57BL6 brains passively stained for 7 and 9 days, respectively).

The following imaging parameters were used to measure the relaxation times: T_1 was calculated from 2D inversion recovery images (TR/TE = 5000/10ms, field of view (FOV) = 1.5 × 1.5 cm^2, matrix 128 × 128, slice thickness = 1 mm, 3 coronal slices equally separated by 2 mm; inversion times (TI) = 13.5, 600, 100, 800, 500, 1000, 2000, 300, 700, 3000, and 400 ms, respectively, for non-stained brains and TI = 0, 13.5, 15, 20, 25, 50, and 75 ms for stained brains). T_2 was evaluated from multislice multiecho images (TR = 5000 ms, FOV = 1.5 × 1.5 cm^2, matrix 128 × 128, slice thickness = 1 mm, 5 coronal slices equally separated by 2 mm, 6 echo times (TE = 12.2 ms for non-stained brains and TE = 7.1 ms for stained brains)). T2* was assessed from multi gradient echo images (TR = 5000 ms, TE = 3.6, 8.4, 13.3, 18.1, 22.9, 27.8, 32.6, 37.5, 42.3, and 47.2 ms, FOV = 2 × 2 cm^2, matrix 128 × 128, slice thickness = 1.1 mm, 1 slice). Parametric T_1, T_2, and T2* maps were generated by fitting pixel intensity values to single exponential curves using Bruker fit package (software: Paravision 1.1). Regions of Interest (ROIs) were positioned in the parietal cortex, temporal cortex, dorsal hippocampus, corpus callosum, and thalamus to evaluate the T_1, T_2, and T2* in these regions.

Three-Dimensional Images of Passively Stained Brains

Two sets of T2*-weighted (T2*w) 3D gradient echo images were recorded for all the brains on which we measured relaxation times ($n = 2$ for non-stained brains, $n = 7$ for stained brains) and also for one additional fixed brain stained for 7 days, for which we did not measure relaxation times (in order to reduce the delay between the inclusion in agar and 3D imaging). The imaging parameters used for these images were TE = 10 and 20 ms, TR = 100 ms, alpha = 90°, FOV = 1.6 × 1.2 × 0.75 cm, matrix = 256 × 256 × 128, resolution = 63 × 47 × 59 μm^3, signal averaging (NA) = 8 to 10, imaging time = 7 to 9 h.

Another experiment was designed to directly compare contrast to noise ratios in passively stained and non-stained tissues. Fixed brains were split into their two hemispheres. One hemisphere was stained for approximately 1 week while the contralateral hemisphere was kept in 10% buffered formalin. The two hemispheres were then embedded together in the agar gel and were imaged with the above 3D imaging protocols. This experiment was applied to the brains of 3 C57BL6, 2 PS1, and 2 APP/PS1 mice.

Finally, the staining and 3D imaging protocols were also applied to fresh tissues to evaluate the effect of brain fixation on the staining protocol. For this experiment 1 C57BL6, 2 PS1, and 2 APP/PS1 animals were sacrificed by cervical dislocation. Their brains were rapidly extracted and one hemisphere was processed by passive staining and maintained in the contrast agent for 1 week while the other hemisphere was fixed in 10% buffered formalin.

Neuropathology

After imaging, brains were cut into 40 μm-thick coronal sections on a freezing microtome. Adjacent sections were processed for Nissl and Congo-red stainings (see (14)). A third batch of sections was used to reveal Aβ deposits using Aβ 1–42 immunohistochemistry (polyclonal antibody FCA-3542, gift from F. Checler, dilution: 1:10000; see (15) for details). All slices were then digitized using a Super CoolScan 8000 ED high-resolution scanner (Nikon, Champigny sur Marne, France).

Correlation Between MRI and Histology

Digitized Congo-red stained histologic sections from passively stained hemispheres of APP/PS1 animals were processed using Photoshop Software (Adobe, San Jose, CA, USA). A macro command was written to automatically dilate plaque surfaces on the images and to enhance their contrast with surrounding tissues. It was based on the following stepwise procedure: from RGB images, the red channel was subtracted from the green channel to eliminate dust and scratches. The auto-levels function was then applied to contrast the image that was finally video-inverted to facilitate matching with MR images. Histologic sections displaying fiducial landmarks, like peripheral artifacts (such as cortical notches), well delimited anatomic structures (e.g., hippocampus, blood vessels), and amyloid

deposits, were then selected to compare to MR images. The MR images were zero-filled to a matrix of 512 × 512 × 256 (thus leading to a digital resolution of 31 × 23 × 29 μm^3) for better comparison with histologic sections, and the zero-filled 3D MRI datasets were virtually sliced at various angles and depths using the "Display" freeware (http://www.bic.mni.mcgill.ca) until the MRI slicing plane that best fitted the chosen histologic landmarks was identified.

RESULTS

Relaxation Times in Control Brains

T_1, T_2, and T2* relaxation times decreased rapidly after immersion of the brains in the contrast agent. For example, T_1 ranged from 700 to 943 ms before staining and decreased to values lower than 80 ms after 1 day in the contrast agent. Relaxation times were stabilized to very low values after 3 days of immersion (Fig. 1a; Table 1).

After inclusion of the brains in the agar gel, T_1, T_2, and T2* relaxation times remained low for at least 30 h. During the first 10 hours in the gel, a slight T_1 (Fig. 1b) and T_2 (data not shown) increase was noticed for most brain structures. During that period, a slight T2* increase was detected only for some structures, such as the hippocampus (Fig. 1c). After 20 h in the gel, T_1 and T_2 differences between tissues were reduced but T2* values of the various tissues were still different (Figs. 1b, 1c).

Three-Dimensional Images of Control Brains

Images from unstained control brains were very poorly contrasted and displayed a low signal to noise ratio (Fig. 2a). Image signal to noise ratio and contrast were improved after the passive staining protocol (Figs. 2b, 2c). The contrast improvement could mainly be explained by signal decrease within the white matter and thalamus, i.e., in the structures that had the shortest T2* values. This effect was more obvious on long TE than on short TE images, which is also consistent with a T2* effect.

The contrast in the stained structures was similar whether the staining protocol had been applied on whole fixed brains (Fig. 2b), fixed hemispheres (Fig. 2c), or fresh hemispheres (data not shown). In addition, we noticed that, for the protocol on hemispheres, some contrast increase, with respect to whole unstained brains, was also observed in unstained hemispheres (Fig. 2c). This was presumably due to diffusion of the contrast agent from stained to unstained hemispheres when split brains were enclosed together.

Plaque Detection in APP/PS1 Mouse Brains

Images from APP/PS1 animals revealed numerous hypointense spots in the cortical areas, hippocampus, and subiculum of the stained hemispheres (Fig. 3). Similar spots were not visible in the non stained APP/PS1 brains nor in the stained brain of control C57BL6 or PS1 mice (data not shown). Older APP/PS1 animals displayed a wider spatial distribution of the spots and a higher spot density (Fig. 3). On long TE images, the spots were larger and more numerous than on short TE images (Figs. 3, 4), so that in older animals, tissues such as the hippocampus or the cortex had a "bread-crumb" or mottled aspect (Fig. 3). As expected (13), histologic studies revealed worsening and spreading of amyloid deposition with aging. For example, in a 28-week-old animal, amyloid deposits were mainly located in the subiculum (Fig. 3a), while in a 39-week-old animal the amyloid deposits were localized in the subic-

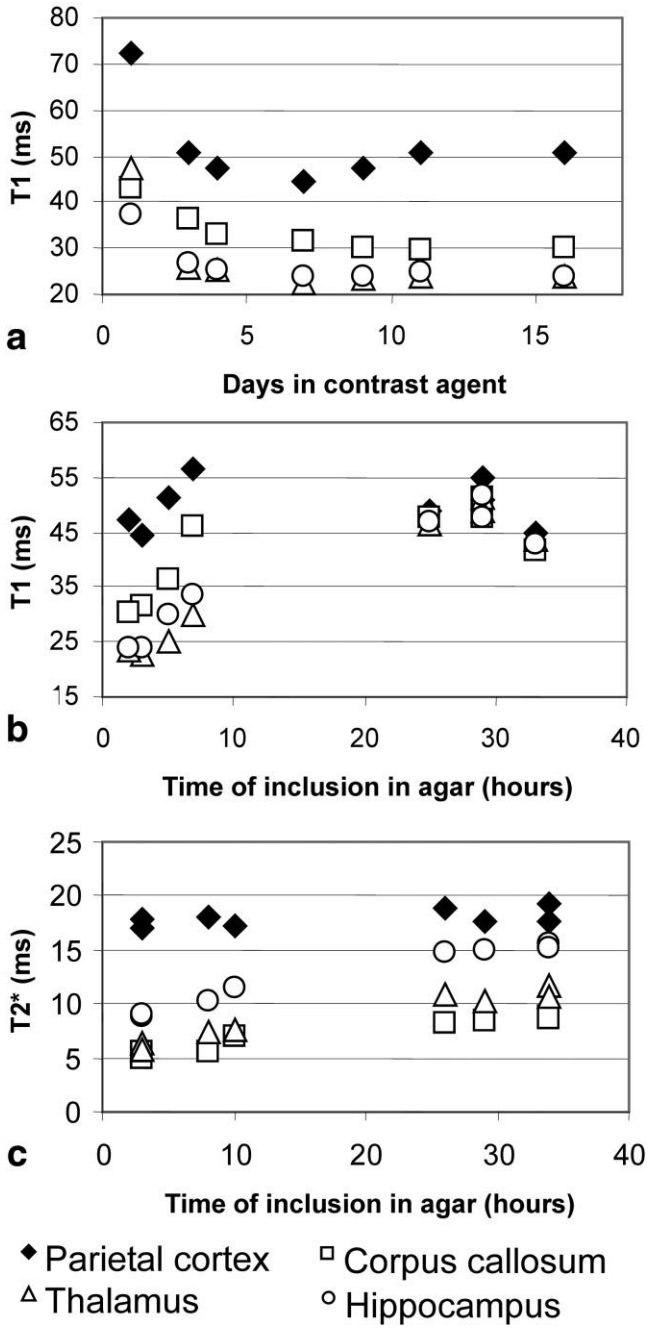

FIG. 1. (**a**) Follow-up of T_1 signal in various brain regions as a function of the time of immersion in the passive staining solution. After 1 day T_1 relaxation times were already short. They were stabilized after 3 days of immersion. T_1 (**b**) and T2* (**c**) evolutions as a function of time spent in the agar gel. A slight T_1 increase was noticed during the first 10 h and a reduction of T_1 difference between brain regions was detected after 20 h of inclusion. T2* differences between tissues persisted even after long inclusion times.

Table 1
Relaxation Times (ms) in Various Unstained and Stained Brain Structures of C57BL6 Mice (4 to 9 days after immersion in the contrast agent ($n = 3$))

	Unstained brains			Stained brains		
	T_1	T_2	T_2^*	T_1	T_2	T_2^*
Parietal cortex	871 ± 62	83 ± 4	42 ± 1	46 ± 1	30 ± 1	17 ± 0
Temporal cortex	943 ± 24	92 ± 0	49 ± 2	46 ± 1	33 ± 1	17 ± 1
Hippocampus	888 ± 20	86 ± 1	46 ± 2	24 ± 0	19 ± 0	9 ± 1
Corpus callosum	700 ± 31	69 ± 1	30 ± 2	31 ± 1	19 ± 1	6 ± 0
Thalamus	751 ± 0	70 ± 1	40 ± 2	24 ± 1	17 ± 0	7 ± 0

ulum, hippocampus, and cortical areas (Fig. 3b). We found that, for a given animal, the spot location and density were similar to that of histologically assessed amyloid deposits (Fig. 4). Moreover, several individual spots visible on the MR images could be matched with the amyloid deposits detected histologically, either by histochemistry or immunohistochemistry (Figs. 3, 4). It is notable that some rare hypointense structures could also be matched with blood vessels (Fig. 3).

DISCUSSION

We implemented a so-called "passive staining" protocol dedicated to the optimization of μMR histology of formalin fixed brains. It is based on the immersion of the brain in a solution of Dotarem®, a widely available contrast agent. This protocol improved the contrast to noise ratio of high resolution 3D gradient echo brain images for amyloid-free animals. Notably, in long TE images, contrast was highly improved between isocortical/hippocampal regions and other brain structures. In addition, we found no marked signal difference when the staining protocol was concomitantly applied with fixative agents on fresh brains or on previously fixed samples. This suggests that it can be used with good efficiency on fixed samples, which are the most widely available in histologic brain banks.

Enhancement of post-mortem images by gadolinium-based contrast agents has already been reported in previous studies where the animals were intracardiacally perfused with a solution of fixative associated with the contrast agent, a protocol called "active staining" (11) or "contrast enhanced MRI" (12). Because of the perfusion protocol, the contrast agent was expected to accumulate within the intravascular space and the contrast-enhancement was, in part, supposed to be related to local modification of the microvasculature. In our study, the contrast agent could only penetrate within the brain by passive diffusion mechanisms.

Estimation of the relaxation times in fixed brains, with and without passive staining protocols, explained the signal modifications. First, there was a rapid and massive T_1, T_2, and T2* decrease in all the evaluated regions of passively stained brains as compared to unstained brains. This suggests that the contrast agent diffused largely in all brain structures after passive staining. T_1 reduction in all brain areas led to overall signal to noise improvement. The shorter T2* values in white matter and subcortical structures with respect to cortex and hippocampus could explain the higher contrast between these structures and the fact that this contrast was more pronounced on long TE images.

Follow-up of relaxation times for more than 30 h after the brains were embedded in the agar gel revealed that T_1, T_2, and T2* values remained low. T2* differences between tissues were still observed even after long periods of inclusion, which implies that the contrast was maintained even when 3D images of the brains were recorded up to 30 h after the inclusion in agar. However, in practice, as

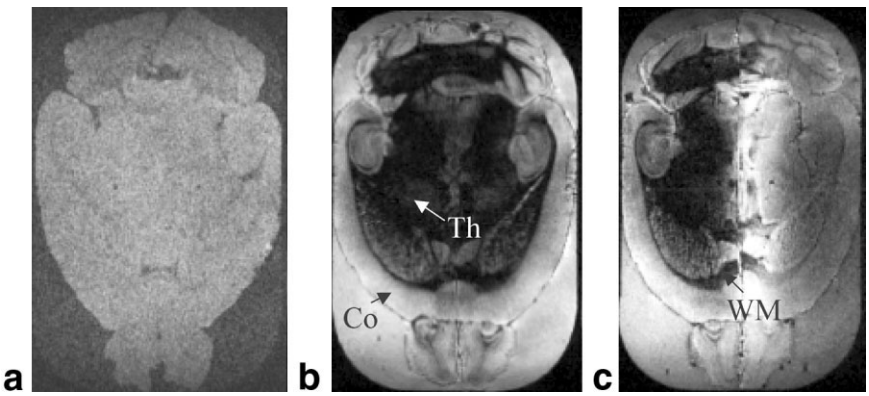

FIG. 2. Evaluation of passive staining protocols in the brain of C57BL6 mice (TR = 100 ms; TE = 20 ms, alpha = 90°). Fixed brains imaged without passive staining (**a**) were poorly contrasted and had a low signal to noise ratio. (**b**) shows a fixed brain stained by passive staining. (**c**) The left hemisphere (right side of images) was fixed by 10% buffered formalin. The right hemisphere (left side of images) was stained by passive staining (after fixation by 10% buffered formalin). After passive staining, the signal was reduced in the white matter (WM) and subcortical regions, such as the thalamus (Th). Other abbreviation: Co: Cortex.

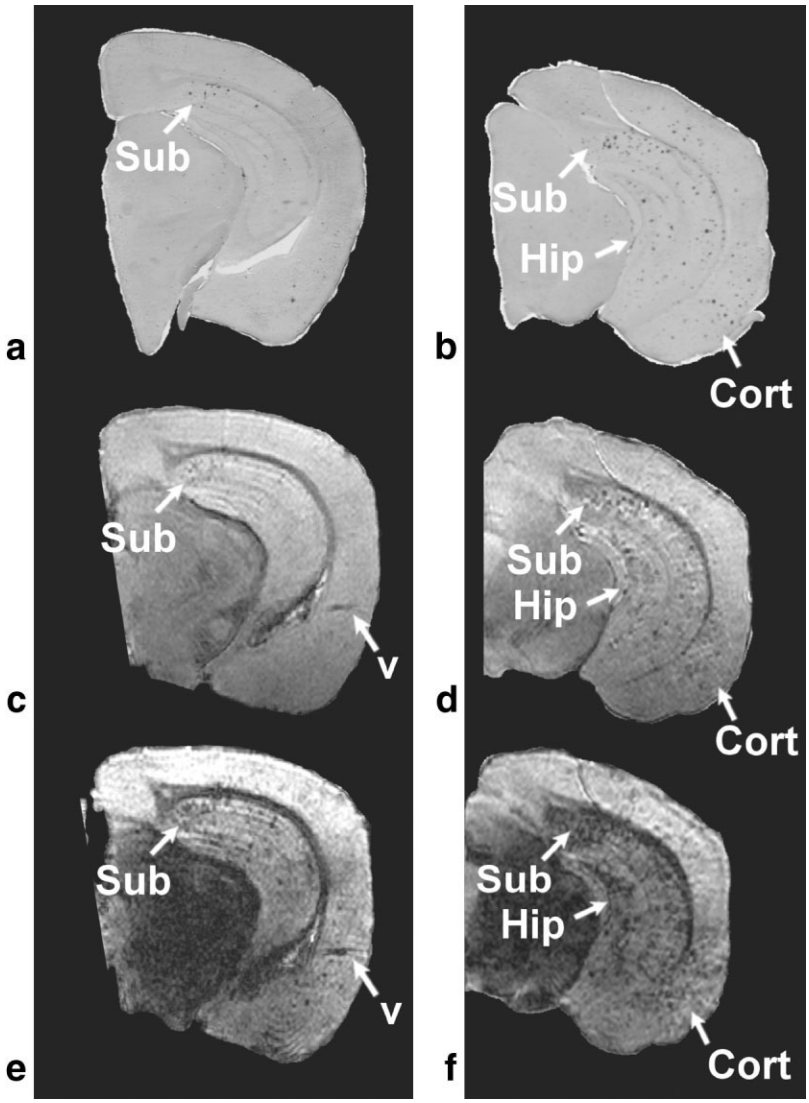

FIG. 3. Amyloid deposits on Congo-red histologic sections (**a**, **b**) compared to hypointense spots on matched MR images from passively stained hemispheres of APP/PS1 mice (**c**, **d**: TE = 10 ms; **e**, **f:** TE = 20 ms). Amyloid deposits in the 28-week-old animal (a, c, e) were mainly located in the subiculum (Sub). Amyloid deposits in the 39-week-old animal (b, d, f) were located in the subiculum (Sub), the hippocampus (Hip), and the cortex (Cort). Note also the lower contrast between the cortex/hippocampus and white matter or subcortical regions in short TE images as compared to long TE images. Other abbreviation: v: blood vessel.

there is some diffusion of the contrast agent into the gel, imaging should be performed as early as possible after inclusion. In addition, we found that after 3 days of staining, relaxation times and contrast were rather stable for at least 15 days, making this protocol robust and easy to handle.

Application of the passive staining protocol to APP/PS1 brains revealed hypointense spots on T2*w MR images. They were visible whatever the TE, but were darker and larger in long TE images. Several results suggest that they correspond to amyloid deposits: (1) The spots were only detected in the brains of APP/PS1 animals and were absent from the brain of control or PS1, amyloid deposit free animals. (2) The spots were localized in areas that are known to display amyloid deposits, such as the subiculum, the hippocampus, and the cortex. Moreover, the topographical distribution and the density of spots were age-dependent, as expected from known neuropathological data, and the spreading of MRI-detected spots was similar to that of histologically assessed amyloid deposits. (3) The spots we identified appear similar to the ones previously described to be amyloid deposits in other MR studies in mice (4,5,8,10). (4) Spots from MR images and plaques from immunostained or histochemically Congo-red stained brain slices were colocalized following matching reconstructions. As in all studies that have attempted to colocalize MRI spots and histologically detected amyloid deposits, there were several spots and plaques that could not be matched. This might be related to the different thickness of histologic sections (40 μm) and MRI slices (approximately 60 μm) and partial volume effects, or limitations in precision of co-registration. Imperfect matching between plaques and spots can also originate from hypointense structures corresponding to blood vessels, as previously described (6). Such artifacts can be suppressed by peri-mortem intracardiac perfusion of the animals to remove the blood from the brain. However, in our study, despite the lack of such perfusion, only a few blood vessels were colocalized with MRI-detected spots.

The increased signal to noise ratio in the cortex and hippocampus from passively stained hemispheres, due to T_1 reduction in the tissues, contributed to senile plaque detection by increasing the signal to noise ratio in the tissues surrounding the plaques. However, as suggested by

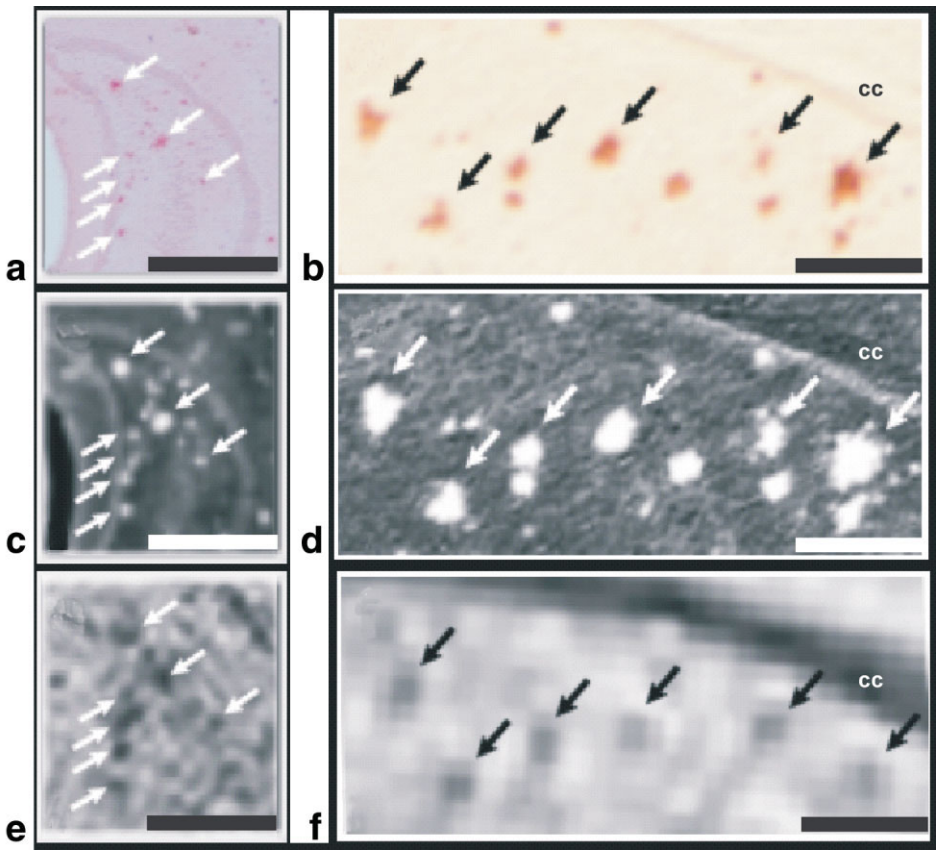

FIG. 4. Comparison of MRI hypointense spots (**e**: TE = 20 ms; **f**: TE = 10 ms) and amyloid deposits as detected by Congo-red staining (image at the level of the dentate gyrus (**a**, **c**)) and immunohistochemistry (image at the level of the CA1 region of the hippocampus (**b**, **d**)). Frames a and b show a non-modified image of the plaques from a histologic section. Images c and d are processed images corresponding to photographs a and b. Image processing slightly enlarged the size of the plaques and inverted the contrast so that plaques are white. Scale bars: 500 μm for a, c, and e; 250 μm for b, d, and f. Other abbreviation: cc: corpus callosum.

the larger size of the plaques on long TE images compared to short TE images, T2* effect was the main contrast generating mechanism for detection of individual plaques. This T2* effect was probably related to the presence of local susceptibility gradients in the plaque vicinity. They can be explained as follows: Because the gadolinium-based contrast agent is a hydrophilic molecule (16) and because the beta sheeted, congophilic, amyloid deposits are hydrophobic (2), one expects that gadolinium concentration in amyloid deposits will be lower than in surrounding tissues. The lack of free water and gadolinium in plaques should lead to local susceptibility differences with surrounding tissues and, thus, to the T2* effect allowing detection of individual plaques.

The different patterns of the plaques on short and long TE images could be used to optimize their detection as a function of amyloid staging. Long TE images, in which plaques were larger/darker than in short TE images, were well suited to identify the plaques in young animals with a low amyloid load. On the other hand, in old animals with heavy amyloid burden, cortex and hippocampus had a "bread-crumb" aspect on long TE images. This was related to the convergence of large dark spots. Consequently, for old animals, individual plaques could be better identified on short TE images.

A few other methods have already been reported to detect amyloid deposits in vivo by MRI. Indeed, methods without contrast agents are based on the detection of endogenous iron that is associated with plaques in aged animals (5,8). However, because not all the plaques spontaneously display iron deposits, it is predictable that the future of senile plaque imaging by MRI will be based on contrast agents (4,5,10,17). To this regard, it is important to evaluate new procedures that can help to detect amyloid deposits. Our study shows that, in addition to direct amyloid labeling, strategies for senile plaque imaging may also be based on the labeling of brain tissues that surround the plaques, for example, by decreasing their T_1.

In conclusion, we present a novel MR-histology method that allows detection of amyloid-β deposits on post-mortem samples. This method relies on the use of a non specific, widely available, contrast agent and can thus easily be performed in any MR laboratory, even using relatively low field spectrometers (4.7T) to create 3D maps of plaques in the brain. This method will be useful to validate, on a 3D basis, the ability of new in vivo MR or PET protocols to detect amyloid-β deposition. Moreover, as our method leaves the brain intact, the sample can be subsequently processed by other methods.

ACKNOWLEDGMENTS

We thank the Sanofi-Aventis Neurodegenerative Disease Group for the generous gift of the animals that were involved in this study, F. Francis for reading and correcting this manuscript, and M. Gregorio and K. Yamada for help in image registrations.

REFERENCES

1. Jellinger KA, Bancher C. Neuropathology of Alzheimer's disease: a critical update. J Neural Transm Suppl 1998;54:77–95.

2. Soto C. Unfolding the role of protein misfolding in neurodegenerative diseases. Nat Rev Neurosci 2003;4:49–60.
3. Dhenain M, Ruffins SW, Jacobs RE. Three-dimensional digital mouse atlas using high resolution MRI. Dev Biol 2001;232:458–470.
4. Zaim Wadghiri Y, Sigurdsson EM, Sadowski M, Elliott JI, Li Y, Scholtzova H, Tang CY, Aguilnaldo G, Pappolla M, Duff K, Wisniewski TM, Turnbull DH. Detection of Alzheimer's amyloid in transgenic mice using magnetic resonance microimaging. Magn Reson Med 2003;50: 293–302.
5. Jack CR, Jr., Garwood M, Wengenack TM, Borowski B, Curran GL, Lin J, Adriany G, Grohn OH, Grimm R, Poduslo JF. In vivo visualization of Alzheimer's amyloid plaques by magnetic resonance imaging in transgenic mice without a contrast agent. Magn Reson Med 2004;52:1263–1271.
6. Dhenain M, Privat N, Duyckaerts C, Jacobs RE. Senile plaques do not induce susceptibility effects in T2*-weighted MR microscopic images. NMR Biomed 2002;15:197–203.
7. Benveniste H, Einstein G, Kim KR, Hulette C, Johnson GA. Detection of neuritic plaques in Alzheimer's disease by magnetic resonance microscopy. P Natl Acad Sci USA 1999;96:14079–14084.
8. Lee SP, Falangola MF, Nixon RA, Duff K, Helpern JA. Visualization of beta-Amyloid plaques in a transgenic mouse model of Alzheimer's disease using MR microscopy without contrast reagents. Magn Reson Med 2004;52:538–544.
9. Vanhoutte G, Dewachter I, Borghgraef P, Van Leuven F, Van der Linden A. Noninvasive in vivo MRI detection of neuritic plaques associated with iron in APP[V717I] transgenic mice, a model for Alzheimer's disease. Magn Reson Med 2005;53:607–613.
10. Poduslo JF, Wengenack TM, Curran GL, Wisniewski T, Sigurdsson EM, Macura SI, Borowski BJ, Jack CR, Jr. Molecular targeting of Alzheimer's amyloid plaques for contrast-enhanced magnetic resonance imaging. Neurobiol Dis 2002;11:315–329.
11. Johnson GA, Cofer GP, Gewalt SL, Hedlund LW. Morphologic phenotyping with MR microscopy: the visible mouse. Radiology 2002;222: 789–793.
12. Benveniste H, Kim K, Zhang L, Johnson GA. Magnetic resonance microscopy of the C57BL mouse brain. NeuroImage 2000;11:601–611.
13. Blanchard V, Moussaoui S, Czech C, Touchet N, Bonici B, Planche M, Canton T, Jedidi I, Gohin M, Wirths O, Bayer TA, Langui D, Duyckaerts C, Tremp G, Pradier L. Time sequence of maturation of dystrophic neurites associated with Ab deposits in APP/PS1 transgenic mice. Exp Neurol 2003;184:247–263.
14. Delatour B, Guegan M, Volk A, Dhenain M. In vivo MRI and histological evaluation of brain atrophy in APP/PS1 transgenic mice. Neurobiol Aging. In press (doi:10.1016/j.neurobiolaging. 2005.04.011).
15. Delatour B, Blanchard V, Pradier L, Duyckaerts C. Alzheimer pathology disorganizes cortico-cortical circuitry: direct evidence from transgenic animal models. Neurobiol Dis 2004;16:41–47.
16. Tweedle MF. Physicochemical properties of gadoteridol and other magnetic resonance contrast agents. Invest Radiology 1992;27 Suppl 1:S2–6.
17. Higuchi M, Iwata N, Matsuba Y, Sato K, Sasamoto K, Saido TC. (19)F and (1)H MRI detection of amyloid beta plaques in vivo. Nat Neurosci 2005;8:527–533.